Linear Trends and Closures of 10-yr Observations of AIRS Stratospheric Channels

FANG PAN AND XIANGLEI HUANG

Department of Climate and Space Sciences and Engineering, University of Michigan, Ann Arbor, Michigan

L. LARABBE STROW

Department of Physics, University of Maryland, Baltimore County, Baltimore, Maryland

HUAN GUO

UCAR Visiting Scientist Programs, NOAA/Geophysical Fluid Dynamics Laboratory, Princeton, New Jersey

(Manuscript received 17 June 2015, in final form 26 August 2015)

ABSTRACT

The Atmospheric Infrared Sounder (AIRS) level-1b radiances have been shown to be well calibrated (~0.3 K or higher) and have little secular drift (~4 mK yr^{-1}) since operation started in September 2002. This paper investigates the linear trends of 10 years (2003–12) of AIRS global-mean radiances in the CO_2 ν_2 band that are sensitive to emissions from the stratosphere (stratospheric channels). AIRS lower-stratospheric channels have a cooling trend of no more than 0.23 K $decade^{-1}$ whereas the midstratospheric channels consistently show a statistically significant cooling trend as large as 0.58 K $decade^{-1}$. The 95% confidence interval for the trend is ~±0.20 K $decade^{-1}$. Two sets of synthetic AIRS radiances are computed using the principal component–based radiative transfer model (PCRTM), one based on a free-running GFDL Atmospheric Model, version 3 (AM3), over the same period and one based on ERA-Interim. The GFDL AM3 simulations overestimate the cooling trends in the mid- to upper-stratospheric channels but slightly underestimate them in the lower-stratospheric channels. The synthetic radiances based on ERA-Interim, however, have statistically significant positive trends at virtually all stratospheric channels. This confirms the challenge to the GCM modeling and reanalysis community to create a better simulation or assimilation of the stratospheric climate. It is shown that the linear trends in AIRS radiances can be reproduced to a large extent by the spectral radiative kernel technique and the trends from the AIRS L2 temperature retrievals and from the change of CO_2. This suggests a closure between AIRS L1 radiances and L2 retrievals and the potential merit of AIRS data in studies of stratosphere changes.

1. Introduction

Stratospheric cooling over last several decades, especially its relation with global warming, has been extensively studied using both observations and numerical models. The observational datasets used in such trend studies include radiosonde observations as well as microwave observations from multiple satellites, namely the MSU (Microwave Sounding Unit), AMSU (Advanced Microwave Sounding Unit), and SSU (Stratospheric Sounding Unit). These observations inevitably suffer from various issues such as the calibration of radiometers, the drift of orbits, and the stability of instruments. The cooling trend is detectable from such satellite observations, although considerable uncertainties still exist in the estimation of magnitudes (Ramaswamy et al. 2001; Seidel et al. 2011; Thompson et al. 2012, and references therein). A large amount of effort then had to be invested in making these datasets into climate-quality data records, as discussed by Zou et al. (2006) and Zou and Wang (2009, 2010, 2011) and the RSS (Remote Sensing Systems) team (Mears and Wentz 2009; Mears et al. 2011). Climate model simulations are also useful in such studies, especially for the detection and attribution studies (e.g., Shine et al. 2003; Ramaswamy et al. 2006; Forster et al. 2011). Reanalyses, on the other hand, suffer from issues such as data inhomogeneities and time-dependent biases in observation

Corresponding author address: Prof. Xianglei Huang, Department of Climate and Space Sciences and Engineering, University of Michigan, 2455 Hayward St., Ann Arbor, MI 48109-2143.
E-mail: xianglei@umich.edu

DOI: 10.1175/JCLI-D-15-0418.1

systems, making them not well suited for trend analysis of the stratospheric temperature (Thorne and Vose 2010).

A potentially valuable dataset for investigating stratospheric temperature trend and variability is the Atmospheric Infrared Sounder (AIRS) aboard NASA's *Aqua* satellite launched in 2002 (Pagano et al. 2003; Aumann et al. 2003; Chahine et al. 2006). The AIRS L1b (level 1b) radiances have been shown to be well calibrated and have little secular drift since it started to record hyperspectral radiances in September 2002 (Aumann and Pagano 2008). Given the rich information contained in the AIRS spectrum, more than a decade of global observations with dense sampling patterns, and the good performance in calibration and stability, some meaningful questions can be investigated using the AIRS data, including the following:

1) Can any statistically significant linear trends be detected already from certain AIRS channels that are sensitive to absorptions and emissions in the stratosphere (hereafter, for brevity, referred as stratospheric channels)? Note this is about the linear trend during the period of AIRS observation. Such a linear trend might be attributed to not only anthropogenic climate change but also decadal climate variability (e.g., stratospheric temperature variability due to solar cycle).
2) Are such statistically significant trends, if they exist, consistent with the trends of AIRS L2 (level 2) retrievals? In another word, as far as the trend is concerned, does a closure exist between AIRS L1 and L2 data products, at least in terms of globally averaged quantities?
3) Can free-running climate models forced by observed sea surface temperatures (SSTs) and CO_2 concentrations over the same period reproduce the trends in AIRS stratospheric channels? How about reanalysis?

This study is motivated by above questions and we carry out both data analysis and model simulations to investigate these questions. The rest of the paper is arranged as follows. Section 2 describes AIRS L1b calibrated radiances and L2 retrievals, the GFDL CM3 model, and the ERA-Interim reanalysis data, as well as the spectral radiative kernels. The linear trends of brightness temperatures of stratospheric channels in the CO_2 ν_2 band are shown and discussed in section 3. Section 4 presents conclusions and further discussion.

2. AIRS data and its processing, forward model, and synthetic AIRS radiances

We have processed and archived 10-yr AIRS data from January 2003 to December 2012. As a comparison, synthetic AIRS radiances are simulated using two datasets as input to a radiative transfer model: one is simulations by a free-running Geophysical Fluid Dynamics Laboratory (GFDL) AM3 model forced by the observed SST over the same period, and the other is the European Centre for Medium-Range Weather Forecasts (ECMWF) interim reanalysis (ERA-Interim). This section will introduce the data processing of AIRS radiances, the GFDL AM3 model and ERA-Interim, as well as the radiative transfer tools used in following sections.

a. AIRS measurements and L1b data processing

AIRS is a grating spectrometer with 2378 channels. The spectral coverage is from 3.7 to 15.4 μm with gaps in between. Its resolving power ($\lambda/\delta\lambda$) is 1200, that is, $\sim$0.5 cm^{-1} spectral resolution in the CO_2 υ_2 fundamental band (also known as the 15-μm band). The initial in-flight calibrations estimated a radiometric accuracy of 0.3 K or higher for a target with 250-K brightness temperature (Pagano et al. 2003), as well as a spectral accuracy better than 0.5% of the full width at half maximum of each channel (Gaiser et al. 2003). Aumann et al. (2006) estimated the calibration accuracy to be better than 0.2 K and the stability to be better than 16 mK yr^{-1}. Aumann and Pagano (2008) updated the stability estimate to $\sim$4 mK yr^{-1}. AIRS collects $\sim$3 million spectra per day and can achieve global coverage within 2 days. It has been operating since September 2002. Such accuracy, stability, dense spatial coverage, and long-term record from one single instrument makes AIRS radiances an attractive dataset in the studies of stratospheric variability and trend.

In this study we examine 10 years of AIRS L1b calibrated radiances from January 2003 to December 2012. Following Huang and Yung (2005), we apply quality controls to each AIRS spectrum to detect abnormal channels. For each AIRS scanning cycle, the AIRS spectra within $\pm$5° scanning angle (cos5° = 0.996) are averaged and deemed as a nadir-view spectrum. Such nadir-view spectra are then averaged onto 2.5° longitude by 2° latitude grid boxes. The averaging onto the grid boxes is done separately for the descending node and the ascending node. Then for every 16 days (i.e., the repeating period for the *Aqua* satellite) of observations, results of the descending node and ascending node are equally averaged to attain a 16-day average. By doing this, we can minimize any sampling disparity between the ascending and descending nodes. Figure 1 shows the number of qualified spectra used for average in each grid box for the entire year of 2004. The sampling is essentially uniform for each latitude band within $\pm$81°, beyond which there is no AIRS nadir-view observation. The number of observations increases considerably as the sun-synchronous satellite *Aqua* approaches its north and south boundaries. This is why the numbers of

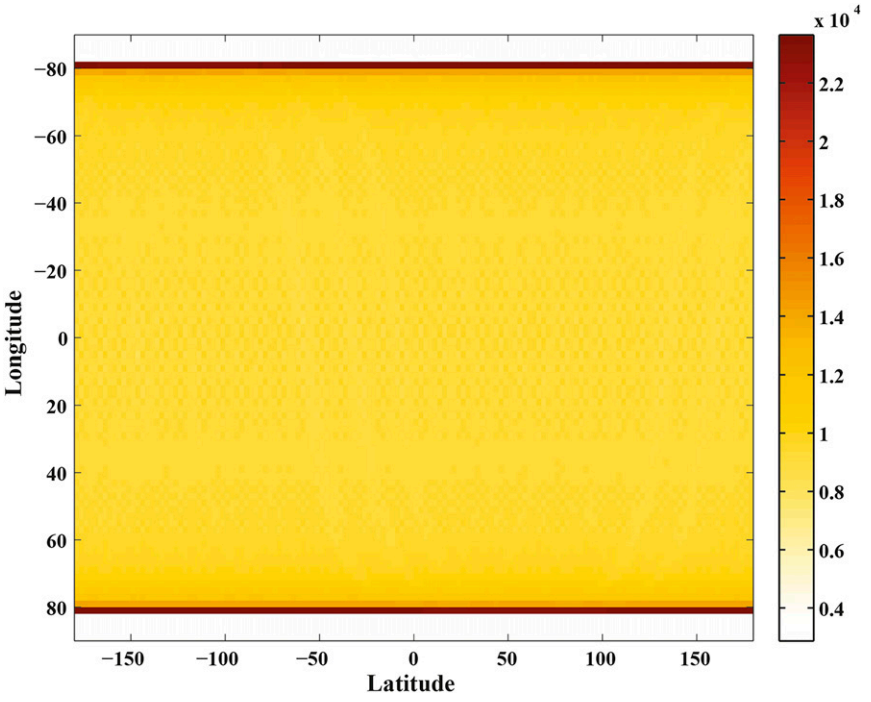

FIG. 1. Number of qualified AIRS spectra used for averaging over the entire year of 2004 in each 2.5° × 2° grid box. The spatial sampling is essentially uniform for each latitude zone.

qualified spectra in 81°–79°S and 79°–81°N latitudinal bands are much larger than the rest.

We focus on global-mean spectra. Moreover, we only focus on channels in the CO_2 15-μm band that are most sensitive to the stratospheric absorption and emission. 50 AIRS channels between 662.5 and 674.9 cm^{-1} are chosen because the peaks of their weighting functions (i.e., the derivation of their transmission function with respect to the pressure) are located in the stratosphere (between 1 and 100 hPa). These channels are affected little by the variations of the tropospheric clouds. We do not choose channels in the CO_2 v_3 fundamental band because they can be affected by solar radiation in addition to thermal emission and absorption, and non-local thermodynamic equilibrilium (LTE) effects sometimes have to be taken into account (DeSouza-Machado et al. 2007). As an example, Fig. 2 shows time series of such global-mean brightness temperature anomalies (deseasonalized deviations from long-term global means) of two stratospheric channels used in our analysis. One channel, 666.02 cm^{-1}, is sensitive to the absorption and emission in the lower stratosphere, and the other channel 667.78 cm^{-1}, is sensitive to the midstratospheric absorption and emission. After the 10-yr mean seasonal cycle is removed, interannual variation can be clearly seen from Fig. 2, especially for the time series of the lower stratospheric channel (Fig. 2a).

b. Synthetic AIRS radiances

In parallel to the AIRS radiance observations, we analyze synthetic AIRS radiances computed using a state-of-the-art radiance simulator (Chen et al. 2013) based on the principal component–based radiative transfer model (PCRTM; Liu et al. 2006). The PCRTM is a fast and accurate radiative transfer model that has been widely used in hyperspectral sounding community. Chen et al. (2013) developed a radiance simulator based on the PCRTM, which is tailored for climate model output as well as reanalysis data and is able to take subgrid variability of clouds into account. More details can be found in Chen et al. (2013).

We generate two sets of synthetic AIRS radiance datasets. One is based on 6-hourly output from a GFDL AM3 model run forced by the observed SST from 2003 to 2012. The AM3 model (Donner et al. 2011) is the latest atmospheric GCM developed by the GFDL. The horizontal resolution is 2.5° longitude by 2° latitude, and it consists of 48 vertical levels with the top at 0.01 hPa. It has 25 levels in the stratosphere and includes online chemistry in both stratosphere and troposphere. The second set of synthetic AIRS radiance is based on the 6-hourly ERA-Interim reanalysis data (Dee et al. 2011). ERA-Interim is the latest reanalysis from the ECMWF. It assimilates a subset of manually selected and quality controlled clear-sky AIRS radiances at up to 210 channels for a typical

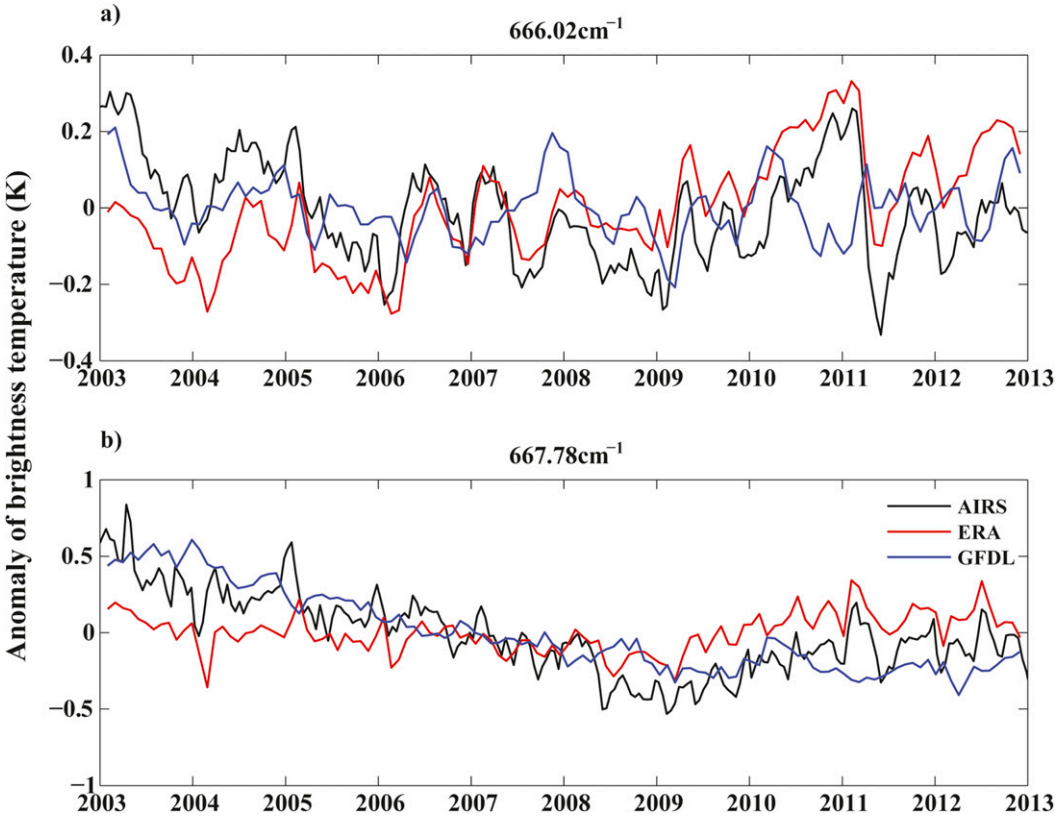

FIG. 2. Time series of global-mean brightness temperature anomalies of two channels: (a) 666.02 cm^{-1} (weighting function peaks at ~66 hPa) and (b) 667.78 cm^{-1} (weighting function peaks at ~2 hPa). Black line is AIRS observation. Red and blue lines show the synthetic AIRS radiance based on ERA-Interim reanalysis data and the GFDL AM3 simulation, respectively.

cloud-free scene over ocean (Dee et al. 2011; McNally et al. 2006). To save the computational cost, the ERA-Interim data are averaged onto a horizontal resolution of 1.5° latitude by 1.5° longitude. ERA-interim has 60 vertical layers with 24 layers in the stratosphere. For both cases, the temperature, humidity, ozone, and cloud profiles are linearly interpolated onto the AIRS trajectories, and then fed into the radiance simulator to generate the AIRS radiances. Then such synthetic AIRS radiances are averaged and processed in the same way as the observed AIRS radiances. CO_2 is assumed to be uniformly mixed and the values are taken from monthly-mean observations compiled by the NOAA Earth System Research Laboratory (Tans and Keeling 2011). The blue and red lines in Fig. 2 show the global-mean radiance anomalies from the synthetic AIRS radiances based on GFDL AM3 model simulation and the ERA-Interim reanalysis, respectively.

c. *Trends estimated using the spectral radiative kernel techniques*

To carry out the "closure" study mentioned in section 1, we will need to compute the trends of synthetic radiances based on the AIRS L2 retrievals. Since the focus here is the global-mean radiances and their trends, we adopt a spectral radiative kernel approach for this investigation. Specifically, the brightness temperature (BT) of a given channel υ at the top of atmosphere (TOA) can be written as the function of atmospheric parameters: $\mathrm{BT}_\upsilon = f_\upsilon(T_s, T_a, \mathrm{H_2O}, \mathrm{CO_2}\ldots)$ and the deviation of the BT_υ from its long-term time-invariant mean state can be expressed as

$$\Delta \mathrm{BT}_\upsilon = \frac{\partial f_\upsilon}{\partial Ts}\Delta T_s + \sum_i \frac{\partial f_\upsilon}{\partial T_a^i}\Delta T_a^i + \sum_i \frac{\partial f_\upsilon}{\partial \mathrm{H_2O}^i}\Delta \mathrm{H_2O}^i + \frac{\partial f_\upsilon}{\partial \mathrm{CO_2}}\Delta \mathrm{CO_2} + \text{Residual}. \quad (1)$$

Its time derivative can be written as

$$\Delta_t \mathrm{BT}_\upsilon = \frac{\partial f_\upsilon}{\partial T_s}\Delta_t T_s + \sum_i \frac{\partial f_\upsilon}{\partial T_a^i}\Delta_t T_a^i + \sum_i \frac{\partial f_\upsilon}{\partial \mathrm{H_2O}^i}\Delta_t \mathrm{H_2O}^i + \frac{\partial f_\upsilon}{\partial \mathrm{CO_2}}\Delta_t \mathrm{CO_2} + \text{Residual}, \quad (2)$$

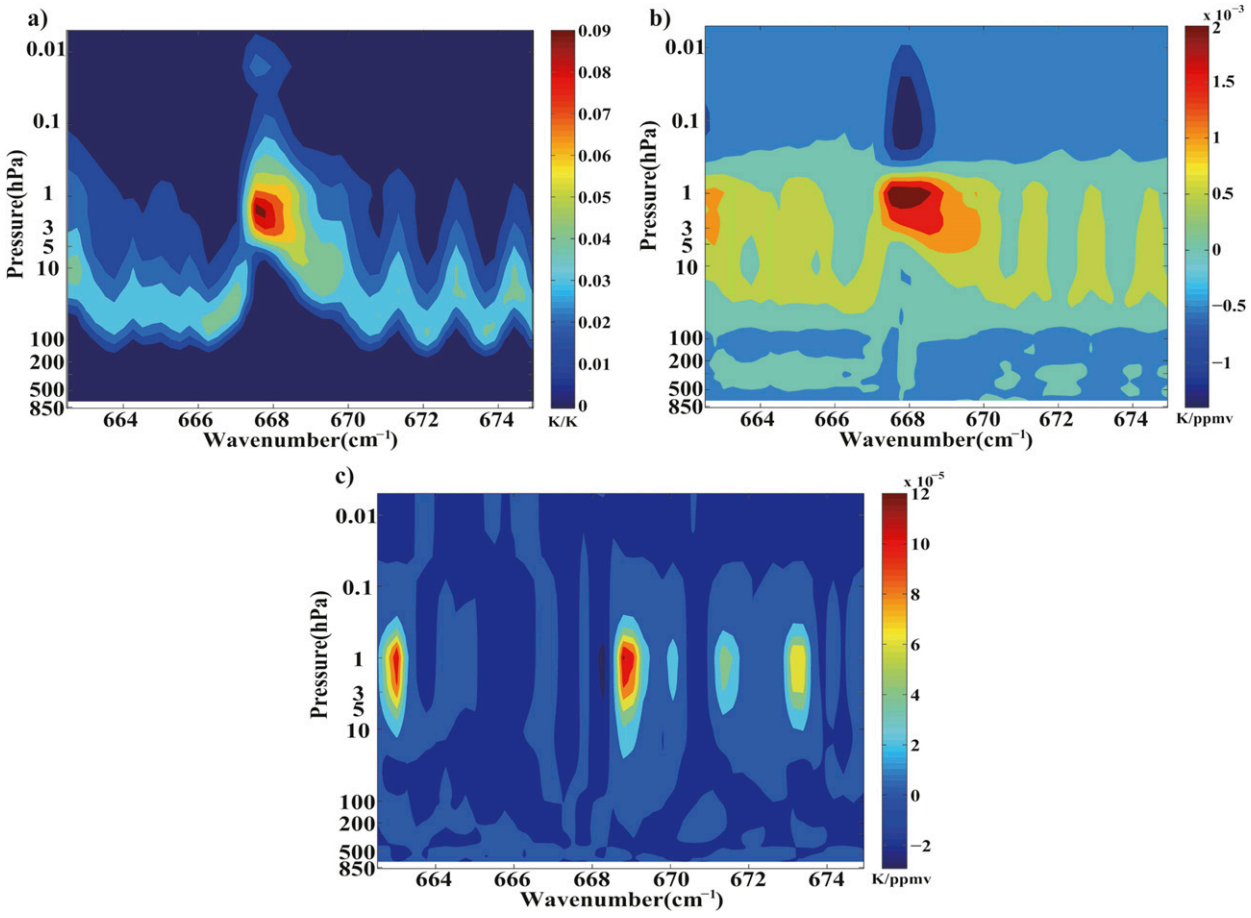

FIG. 3. (a) Global-mean radiative kernel with respect to the air temperature which is expressed as the change of brightness temperature (in K) for 1-K change of air temperature in each vertical layer predefined in the PCRTM. The PCRTM has 100 predefined vertical layers in total. (b) As in (a), but for CO_2 in ppmv. (c) As in (a), but for H_2O in ppmv.

where Δ is the deviation from the mean state (i.e., anomaly) and Δ_t is the first-order derivation with respect to time and $\partial f_v/\partial X$ is the radiative kernel; T_a and T_s denote air temperature and surface temperature, respectively. Superscript i refers to the ith layer in the atmosphere. H_2O and CO_2 refer to the mixing ratios of water vapor and carbon dioxide, respectively. According to Eq. (2), linear trends of temperatures and trace gas mixing ratios can be used to estimate the corresponding trend of BT at an AIRS stratospheric channel as long as the spectral radiative kernel kernels, $\partial f_v/\partial X$, are available.

We follow the approach in Huang et al. (2014) to construct the spectral radiative kernel. Specifically, the spectral radiative kernels are computed using the PCRTM-based radiance simulator for each ERA-Interim grid box; then they are weighted by the cosines of their latitudes and averaged to obtain a set of global-mean radiative kernels. Figure 3 shows the global-mean spectral radiative kernels with respect to air temperatures, CO_2 and H_2O mixing ratios at different pressure levels. Figure 3a and 3b clearly show that the AIRS stratospheric channels examined in this study have little sensitivity to temperatures and CO_2 concentrations below 200 hPa. Figure 3c reconfirms that stratospheric water vapor variations contribute little to the radiance variations in the stratospheric channels within the CO_2 15-μm band. For 1 ppmv variation of H_2O, it can only cause $\sim 1.67 \times 10^{-4}$ K or less change of brightness temperature in the stratospheric channels examined here, which is only $\sim$1.2% or less of the change caused by 1 ppmv variation of CO_2. Moreover, eight years of Microwave Limb Sounder (MLS) measurements (EOS MLS Science Team 2011) indicate that the year-to-year variation of global-mean H_2O mixing ratio between 0.7 and 3.3 hPa is no more than 0.2 ppmv. No statistical significant trends are derivable from the 8 years of MLS data (Nedoluha et al. 2013). Thus, the contribution of water vapor long-term change to the trends of BTs is negligible and we will ignore it in the following discussion.

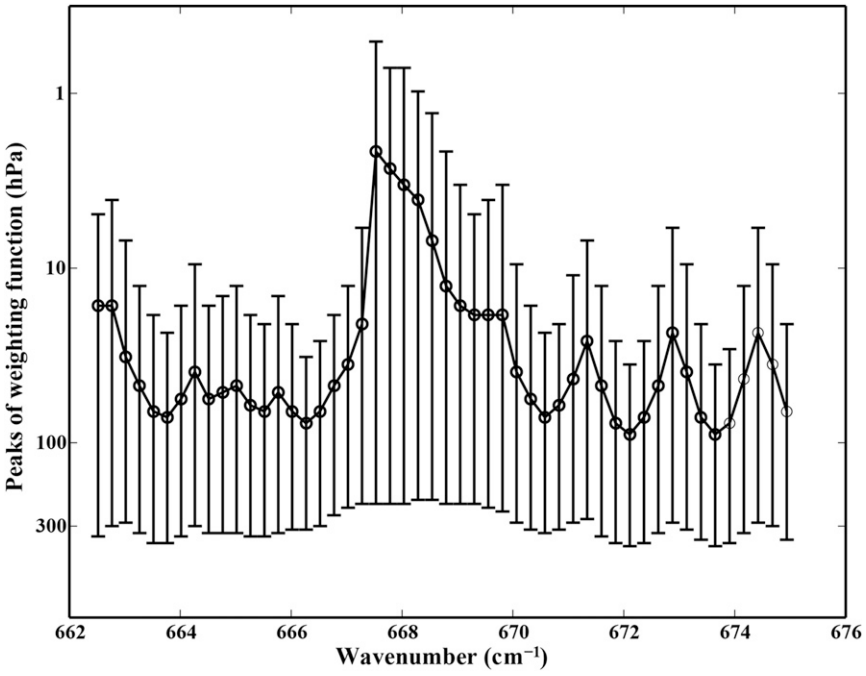

FIG. 4. Peaks of the weighting functions for the AIRS channels in the CO_2 ν_2 band used in this study. Profiles of 1976 U.S. Standard Atmosphere are used in the calculation of the weighting functions. The vertical ticked line indicates the full width of half maximum of the weighting function.

As for the trends of geophysical parameters in Eq. (2), the temperature trend is derived using AIRS L2 temperature retrievals (Chahine et al. 2006). The AIRS L2 temperature retrievals are based on cloud-cleared AIRS radiances and globally averaged linearly variable CO_2 climatology with time throughout the atmosphere. The forward radiative transfer model used in retrieval is different from the radiative transfer model used in this study. Similar to the data processing of AIRS radiances, we average the AIRS L2 temperature retrievals onto 2.5° longitude by 2° latitude grid boxes and then get the monthly-mean temperature profiles on the global scale. L2 temperature retrievals have 28 vertical levels between 1100 and 0.1 hPa with a horizontal resolution of ~45 km. Intensive validation of the AIRS retrievals showed that AIRS retrieval achieves about 1-K root-mean-square (RMS) accuracy over ocean and about 1.7-K RMS accuracy over land (Fetzer et al. 2003; Chahine et al. 2006). CO_2 is assumed to be uniformly mixed over the atmosphere and the monthly-mean concentration of CO_2 is based on the measurements from NOAA Earth System Research Laboratory (Tans and Keeling 2011). Based on the assumptions and the measurements, the linear increment trend of well-mixed CO_2 is 1.95 ppmv yr^{-1} throughout the entire atmosphere. With the radiative kernels and linear trends of temperatures and CO_2 mixing ratios derived, we can use Eq. (2) to calculate linear trends of the brightness temperatures to the first-order approximation, and then compare them with those derived directly from the AIRS L1 radiance records. This is the closure study referred to in section 1.

3. Results

a. Linear trend analysis

The linear trend of the time series of brightness temperature of each stratospheric channel is estimated in following ways: first the mean value is subtracted from the time series and then the time series is deseasonalized by removing the mean seasonal cycle. Finally, the trend is estimated by linear regression. The uncertainty associated with the trend is estimated with the autocorrelation time scale taken into account (Weatherhead et al. 1998).

Figure 4 shows the peaks of weighting functions of the 50 stratospheric channels used in this study, which indicates the pressure level to which the radiance in each channel is most sensitive. The peaks are all in the stratosphere between 100 and 1 hPa. Figure 5 plots the linear trends of the 50 channels derived from AIRS observations with respect to the peak pressure level of their weighting functions. Note that this is for a convenient way of visualizing the results and the ordinate is not the pressure coordinate. The counterparts derived from the synthetic AIRS radiances based on the GFDL AM3 simulation and the ERA-Interim reanalysis are

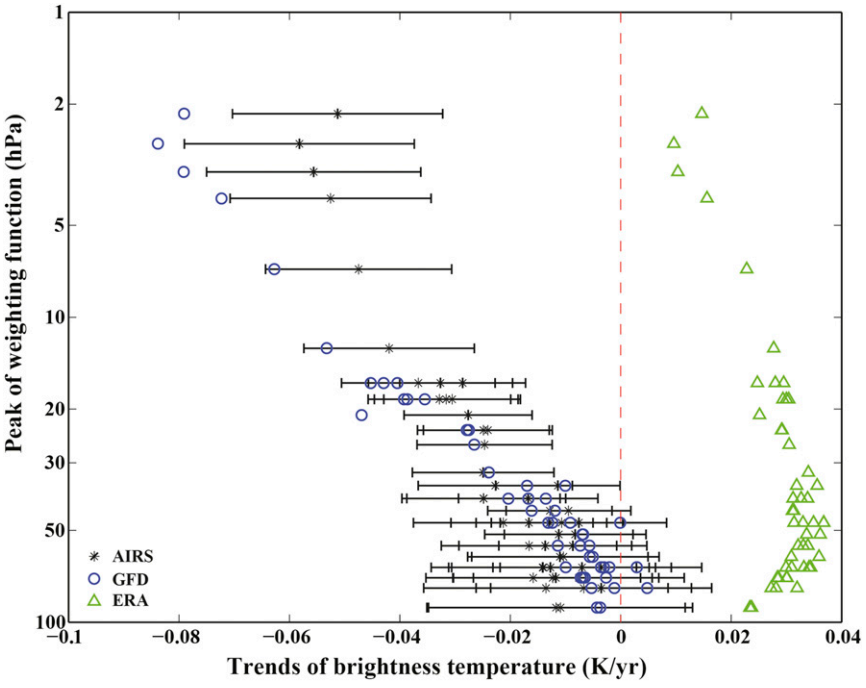

FIG. 5. Black stars are linear trends of brightness temperatures in the AIRS stratospheric channels plotted with respect to the peaks of the weighting functions of the corresponding channels. Black ticked bars denote 95% confidence levels with the correlation time scale taken into account. Blue circles are the linear trends based on the synthetic AIRS radiances computed using the GFDL AM3 simulation output. Green circles are results using ERA-Interim.

shown in the same figure as well. The AIRS channels with peaks above 47 hPa all show statistically significant cooling trends. Furthermore, the higher the peak is, the larger the cooling trend generally is. Between 47 and 30 hPa, BT cooling trend is about 0.1–0.25 K decade^{-1}. Above 10 hPa, the cooling trend is as large as 0.5–0.6 K decade^{-1}. Below 47 hPa, the trend is generally negative at about -0.1 K decade^{-1} but statistically insignificant. Similar trend tendencies are captured by the free-running GFDL AM3 simulation except that the model overestimates the cooling trends above 15 hPa. In contrast, results based on ERA-Interim show statistically significant positive trends in virtually all the stratospheric channels. This could be related to the time-dependent warm biases in the ERA-interim reanalysis data (Dee et al. 2011). Since it is not expected for the meteorological reanalysis to have accurate representation of the secular trend in the stratosphere, we do not investigate the cause of the positive trends of ERA-Interim further.

Given the presence of natural variability, one inevitable question to explore is this: How long it would take for a trend signal to emerge in the presence of natural variability. We estimate the minimum time for detecting secular trend out of the BT time series of the 50 AIRS stratospheric channels using a formula proposed by Leroy et al. (2008b):

$$n = \left[\frac{12s^2}{m_{\rm est}^2}\sigma_{\rm var}^2\tau_{\rm var}\right]^{1/3}(1+f^2)^{1/3}, \qquad (3)$$

where n is the time needed to detect a trend signal, $m_{\rm est}$ is the trend to be detected, s is the signal-to-noise ratio ($m_{\rm est}/\delta m_{\rm est}$), $\tau_{\rm var}$ is the correlation time of natural variability, $\sigma_{\rm var}$ is defined as the standard deviation of the dataset, and f is the measurement uncertainty. We set $s = 5$, the same value used in Leroy et al. (2008b); f is set to zero in our estimation. Given the AIRS radiometric uncertainty is ~0.3 K for a 250-K BT target, and f is ~0.0012, which justifies our choice of simply assuming $f = 0$. The natural variability is obtained from the simulated synthetic AIRS radiance based on the output from a 500-yr control run by the GFDL most recent coupled GCM, the CM3 (Donner et al. 2011). For the stratospheric channels examined here, the natural variability ranges from 0.05 to 0.3 K and the correlation time of natural variability, as defined in Leroy et al. (2008b), varies from 2 to 20 years. Using above information, we compute n for each channel and the results are shown in Fig. 6. The estimated time for trend detection is less than 10 years for all the channels except 666.27 cm^{-1} (weighting function peaks at 77.24 hPa) and 666.52 cm^{-1} (weighting function peaks at 66.13 hPa). Although such

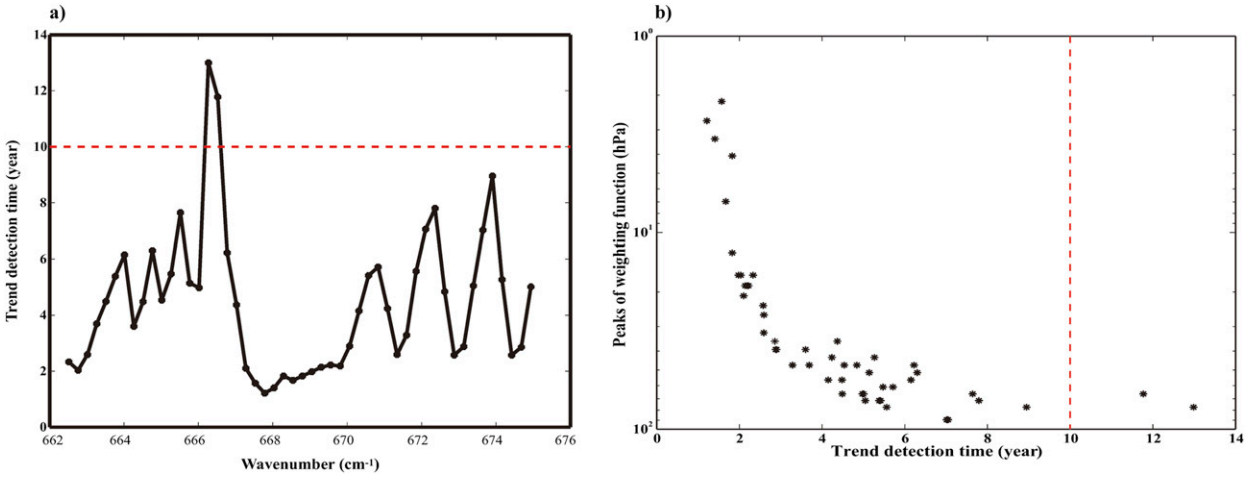

FIG. 6. (a) Time for trend detection in the presence of natural variability for each AIRS stratospheric channel examined here. The natural variability is derived from 500 years of the GFDL CM3 runs and the signal-to-noise ratio is set to 5. (b) As in (a), except that the time for trend detection is plotted with respect to the peak of the weighting function of each the AIRS stratospheric channel.

estimate is based on modeled natural variability and correlation time scale from one particular GCM simulation, Figs. 6a and 6b suggest that statistical significant trends can be derived within a 10-yr time frame for most channels examined here. This is consistent with what is shown in Fig. 5.

b. *Closure study using radiative kernel technique*

As described in section 2d, we use the linear trends of air temperature and CO_2 at all pressure levels together with precomputed spectral radiative kernels to compute the trend in each AIRS stratospheric channel (black line in Fig. 7), as

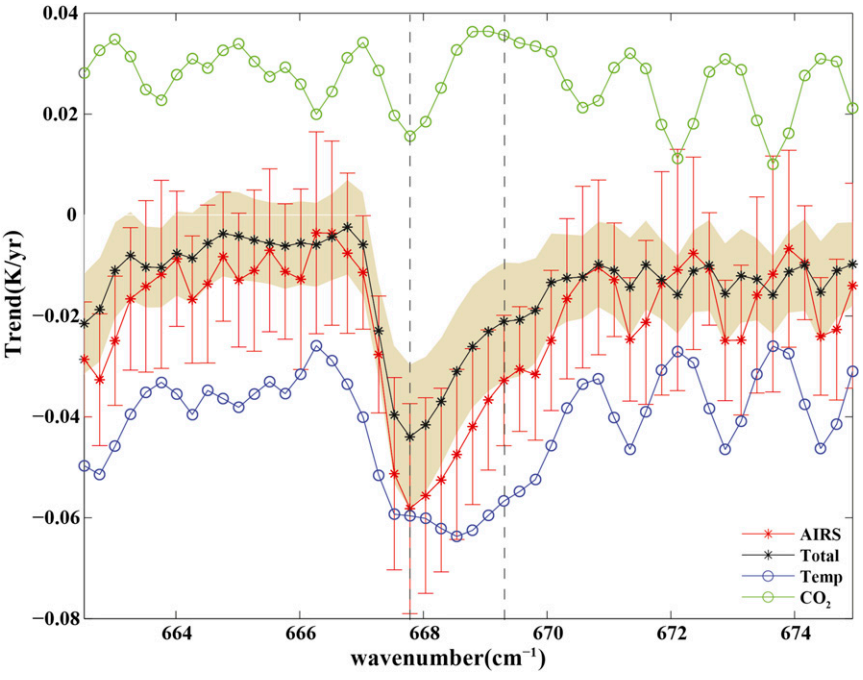

FIG. 7. The BT linear trends derived from AIRS radiance time series are shown as red stars with 95% confidence interval (vertical ticked red line). The BT linear trends estimated using the global-mean spectral radiative kernels and linear trends of surface CO_2 observations and AIRS L2 retrieved temperatures are shown as black stars with 95% confidence interval (yellow shades). The individual contributions of air temperature (blue circles) and CO_2 (green circles) to the estimated BT trends are shown as well. Two vertical black dashed lines denote the spectral region where the observed and estimated BT trends differ the most.

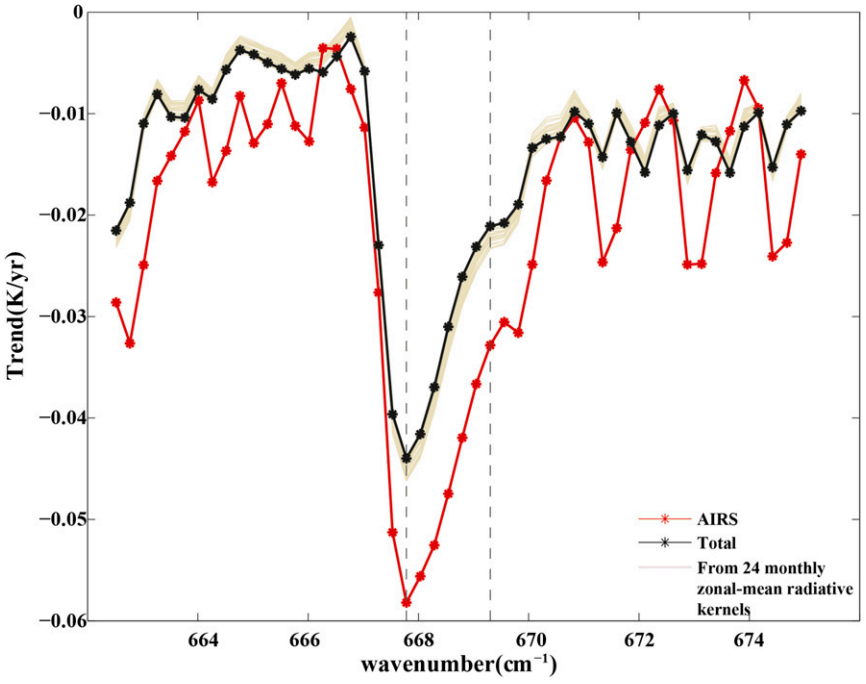

FIG. 8. The BT trends from actual AIRS radiance time series (red) and the BT trends estimated using global-mean spectral radiative kernel in Eq. (2) (black). Gray lines are the global BT trends estimated using 24 different sets of zonal- and monthly-mean spectral radiative kernels for every 2° latitude bin; 12 sets are from the GFDL CM3 simulations and the rest from ERA-Interim. Between the dashed lines is the spectral region we are interested in.

well as the contribution of air temperature and CO_2 to such trends, respectively (blue and green lines in Fig. 7). The trends from actual AIRS radiance time series are plotted in red. The estimated trend using air temperature and CO_2 linear trends falls within 95% confidence interval of the actual AIRS trends for all the stratospheric channels examined here. The good agreement suggests that the AIRS L2 retrievals and surface observations of CO_2 mixing ratio can largely reproduce the BT trends derived from the AIRS L1b radiance time series. The largest discrepancies between actual and computed trends are seen between ~668–670 cm^{-1}, that is, on the Q branch of the CO_2 ν_2 band, where observed BT trends are out of the 95% confidence intervals of the estimated trends using Eq. (2). A couple of possible reasons for the discrepancies in this spectral range are the following:

1) The linear approximation employed in Eq. (2) is not enough to explain the actual trends. The nonlinear terms should be taken into account.
2) There is uncertainty associated with the construction of spectral radiative kernel used in Fig. 7 (e.g., choices of months and years of the input atmospheric profiles, etc.).

As for the first reason, the previous study by Chen et al. (2013) has shown that, at least for the globally average radiances, the linear approximation is a valid approximation for the frequencies examined in this study. As for the second reason, we use following method to quantify the uncertainties associated with the construction of the spectral radiative kernel. We recompute the linear trend in BT using the zonal-mean spectral radiative kernels of an individual month instead of annual and global-mean spectral radiative kernels. Specifically, the zonal-mean spectral radiative kernels and zonal-mean temperature anomalies are used to estimate the zonal trend of BT for every 2° latitude bin, then such zonal-mean BT trend is weighted by the area and averaged to obtain the global-mean BT trend. We construct such zonal-mean kernels based on 12 months of ERA-Interim reanalysis and 12 months of free-running GFDL CM3 simulations, respectively. By doing so, we have 24 estimates of the BT trends in total, which are then used as a measure of uncertainty associated with the construction of the kernels. The results are shown in Fig. 8. Note the spreads in Fig. 8 are solely due to different kernels used in the estimates; the uncertainty of the trends in the AIRS L2 temperature retrievals (the orange shades on Fig. 7) is not included here. It can be seen that the uncertainty due to different ways of constructing spectral radiative kernels has little impact on the final results and cannot be a major reason for the discrepancies between the observed

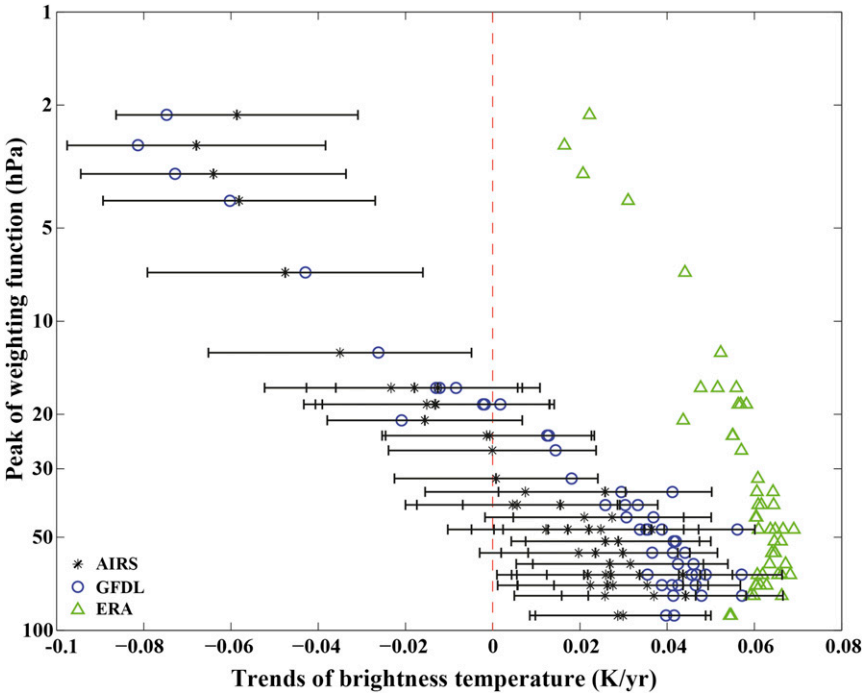

FIG. 9. As in Fig. 5, but for the tropical-mean instead of global-mean trend results.

and estimated BT trends in the stratosphere channels shown in Fig. 7.

Although there are discrepancies in some spectral regions, Figs. 7 and 8 show large consistency between the observed trends based on the AIRS L1b radiances and their counterparts based on the AIRS L2 retrievals and spectral radiative kernels. As far as the global average is concerned, they show that the secular trends of AIRS L1b radiances and L2 temperature retrievals are consistent with each other.

4. Conclusions and discussion

Motivated by the excellent performance of AIRS instrument, we compile 10-yr (2003–12) AIRS L1b radiances and estimate the linear trends of global-mean radiances at 50 stratospheric channels in the CO_2 ν_2 band. For comparison, two sets of synthetic AIRS radiances at these channels are simulated using two different inputs: simulation from a free-running GFDL AM3 model and the ERA-Interim reanalysis. While the results based on the GFDL AM3 model can agree with the observed trends to some extent, the trends based on ERA-Interim have opposite signs compared to the observed ones. This reaffirms that cautions must be taken in the use of reanalysis stratospheric data in the study of trends and variability over multiple years.

Employing the radiative kernel technique, we show that the secular linear trends of the AIRS L1b radiances in these channels can be largely reproduced using AIRS L2 retrievals and surface observations of CO_2 mixing ratios. Although there are discrepancies around ~668–670 cm^{-1} between the L1b trends and the trends based on the L2 retrievals, the general agreements are satisfactory. The discrepancies around ~668–670 cm^{-1} could be due to other reasons, such as the modeling of CO_2 line mixing within this band, undetected spectral shift over such long period, or the breakdown of linearity assumption needed for the radiative kernel analysis.

This study is focused on the conventional linear trend analysis from the actual AIRS radiances. As shown in Fig. 6, the detection of trends in the presence of natural variability can be achieved at many channels using 10 years or less of data. This suggests that formal detection and attribution studies might be possible using the 10+ years of the AIRS L1 radiances, such as the optimal spectral fingerprinting technique in Leroy et al. (2008a). Observationally, careful examinations are warranted to ensure the long-term performance of the AIRS instruments, especially for the possible drift of radiometric or spectral calibrations. On the other side, spectral fingerprints need to be constructed correctly in such detection and attribution studies. One particular challenge would be how to take the actual solar variation into account, as the 11-yr solar cycle can likely affect the stratospheric temperatures (Coughlin and Tung 2004). Besides the global-mean trend analysis, the AIRS data can also be used to study the zonal-mean trends in each latitude or climate zone. An example is given in Fig. 9,

which shows the trends of tropical-mean (30°S–30°N) brightness temperatures in the stratospheric channels. Negative brightness temperature trends in the upper-stratospheric channels are comparable to those of global-mean results in Fig. 5. The trends in the lower-stratospheric channels are slightly positive, opposite to the negative global-mean trends in Fig. 5. This suggests that the extratropics must have negative brightness temperature trends in the lower-stratospheric channels. As for the tropical-mean trends, the GFDL CM3 simulated results agree with AIRS observations within 95% confidence intervals virtually for all the channels. Such latitudinal dependence of brightness temperature trends can potentially help us further understand the observed and simulated meridional circulation change in the stratosphere. Such topics would be the focuses of our follow-up studies.

Acknowledgments. We thank two anonymous reviewers for their thoughtful suggestions and comments. The AIRS level-1b data are obtained from NASA GSFC DAAC and the AIRS L2 data from http://disc.sci.gsfc.nasa.gov/AIRS/data-holdings/by-data-product-V6. The ECMWF ERA-Interim data are from http://apps.ecmwf.int/datasets/data/interim-full-daily/. We thank Dr. X. H. Chen for her help in the early stage of this study. This research is supported by NASA Grants NNX11AE68G and NNX15AC25G awarded to the University of Michigan.

REFERENCES

Aumann, H. H., and T. S. Pagano, 2008: Using AIRS and IASI data to evaluate absolute radiometric accuracy and stability for climate applications. *Atmospheric and Environmental Remote Sensing Data Processing and Utilization IV: Readiness for GEOSS II*, M. D. Golberg et al., Eds., International Society for Optical Engineering (SPIE Proceedings, Vol. 7085), 708504, doi:10.1117/12.795225.

——, and Coauthors, 2003: AIRS/AMSU/HSB on the Aqua mission: Design, science objectives, data products, and processing systems. *IEEE Trans. Geosci. Remote Sens.*, **41**, 253–264, doi:10.1109/TGRS.2002.808356.

——, S. Broberg, D. Elliott, S. Gaiser, and D. Gregorich, 2006: Three years of AIRS radiometric calibration validation using sea surface temperatures. *J. Geophys. Res.*, **111**, D16S90, doi:10.1029/2005JD006822.

Chahine, M. T., and Coauthors, 2006: AIRS: Improving weather forecasting and providing new data on greenhouse gases. *Bull. Amer. Meteor. Soc.*, **87**, 911–926, doi:10.1175/BAMS-87-7-911.

Chen, X., X. Huang, and X. Liu, 2013: Non-negligible effects of cloud vertical overlapping assumptions on longwave spectral fingerprinting studies. *J. Geophys. Res. Atmos.*, **118**, 7309–7320, doi:10.1002/jgrd.50562.

Coughlin, K., and K.-K. Tung, 2004: Eleven-year solar cycle signal throughout the lower atmosphere. *J. Geophys. Res.*, **109**, D21105, doi:10.1029/2004JD004873.

Dee, D. P., and Coauthors, 2011: The ERA-Interim reanalysis: Configuration and performance of the data assimilation system. *Quart. J. Roy. Meteor. Soc.*, **137**, 553–597, doi:10.1002/qj.828.

DeSouza-Machado, S., L. L. Strow, S. E. Hannon, H. E. Motteler, M. Lopez-Puertas, B. Funke, and D. P. Edwards, 2007: Fast forward radiative transfer modeling of 4.3 μm nonlocal thermodynamic equilibrium effects for infrared temperature sounders. *Geophys. Res. Lett.*, **34**, L01802, doi:10.1029/2006GL026684.

Donner, L. J., and Coauthors, 2011: The dynamical core, physical parameterizations, and basic simulation characteristics of the atmospheric component AM3 of the GFDL global coupled model CM3. *J. Climate*, **24**, 3484–3519, doi:10.1175/2011JCLI3955.1.

EOS MLS Science Team, 2011: MLS/Aura Level 2 Water Vapor (H2O) Mixing Ratio, version 003. NASA Goddard Earth Science Data and Information Services Center, accessed February 2014. [Available online at http://disc.gsfc.nasa.gov/datacollection/ML2H2O_V003.html.]

Fetzer, E., and Coauthors, 2003: AIRS/AMSU/HSB validation. *IEEE Trans. Geosci. Remote Sens.*, **41**, 418–431, doi:10.1109/TGRS.2002.808293.

Forster, P. M., and Coauthors, 2011: Evaluation of radiation scheme performance within chemistry climate models. *J. Geophys. Res.*, **116**, D10302, doi:10.1029/2010JD015361.

Gaiser, S. L., H. H. Aumann, D. T. Gregorich, and T. J. Hearty, 2003: In-flight refinement of the radiometric, spectral, and spatial calibration of the atmospheric infrared sounder (AIRS). *Earth Observing Systems VIII*, W. L. Barnes, Ed., International Society for Optical Engineering (SPIE Proceedings, Vol. 5151), 232, doi:10.1117/12.506380.

Huang, X., and Y. L. Yung, 2005: Spatial and spectral variability of the outgoing thermal IR spectra from AIRS: A case study of July 2003. *J. Geophys. Res.*, **110**, D12102, doi:10.1029/2004JD005530.

——, X. Chen, B. J. Soden, and X. Liu, 2014: The spectral dimension of longwave feedback in the CMIP3 and CMIP5 experiments. *Geophys. Res. Lett.*, **41**, 7830–7837, doi:10.1002/2014GL061938.

Leroy, S. S., J. G. Anderson, J. Dykema, and R. Goody, 2008a: Testing climate models using thermal infrared spectra. *J. Climate*, **21**, 1863–1875, doi:10.1175/2007JCLI2061.1.

——, ——, and G. Ohring, 2008b: Climate signal detection times and constraints on climate benchmark accuracy requirements. *J. Climate*, **21**, 841–846, doi:10.1175/2007JCLI1946.1.

Liu, X., W. L. Smith, D. K. Zhou, and A. Larar, 2006: Principal component–based radiative transfer model for hyperspectral sensors: Theoretical concept. *Appl. Opt.*, **45**, 201–209, doi:10.1364/AO.45.000201.

McNally, A. P., P. D. Watts, J. A. Smith, R. Engelen, G. A. Kelly, J. N. Thépaut, and M. Matricardi, 2006: The assimilation of AIRS radiance data at ECMWF. *Quart. J. Roy. Meteor. Soc.*, **132**, 935–957, doi:10.1256/qj.04.171.

Mears, C. A., and F. J. Wentz, 2009: Construction of the Remote Sensing Systems V3.2 atmospheric temperature records from the MSU and AMSU microwave sounders. *J. Atmos. Oceanic Technol.*, **26**, 1040–1056, doi:10.1175/2008JTECHA1176.1.

——, ——, P. Thorne, and D. Bernie, 2011: Assessing uncertainty in estimates of atmospheric temperature changes from MSU and AMSU using a Monte-Carlo estimation technique. *J. Geophys. Res.*, **116**, D08112, doi:10.1029/2010JD014954.

Nedoluha, G. E., R. Michael Gomez, D. R. Allen, A. Lambert, C. Boone, and G. Stiller, 2013: Variations in middle atmospheric water vapor from 2004 to 2013. *J. Geophys. Res. Atmos.*, **118**, 11 285–11 293, doi:10.1002/jgrd.50834.

Pagano, T. S., H. H. Aumann, D. E. Hagan, and K. Overoye, 2003: Prelaunch and in-flight radiometric calibration of the Atmospheric Infrared Sounder (AIRS). *IEEE Trans. Geosci. Remote Sens.*, **41**, 265–273, doi:10.1109/TGRS.2002.808324.

Ramaswamy, V., and Coauthors, 2001: Stratospheric temperature trends: Observations and model simulations. *Rev. Geophys.*, **39**, 71–122, doi:10.1029/1999RG000065.

——, M. D. Schwarzkopf, W. J. Randel, B. D. Santer, B. J. Soden, and G. L. Stenchikov, 2006: Anthropogenic and natural influences in the evolution of lower stratospheric cooling. *Science*, **311**, 1138–1141, doi:10.1126/science.1122587.

Seidel, D. J., N. P. Gillett, J. R. Lanzante, K. P. Shine, and P. W. Thorne, 2011: Stratospheric temperature trends: Our evolving understanding. *Wiley Interdiscip. Rev.: Climate Change*, **2**, 592–616, doi:10.1002/wcc.125.

Shine, K. P., and Coauthors, 2003: A comparison of model-simulated trends in stratospheric temperatures. *Quart. J. Roy. Meteor. Soc.*, **129**, 1565–1588, doi:10.1256/qj.02.186.

Tans, P., and R. Keeling, 2011: Trends in atmospheric carbon dioxide. NOAA Earth Systems Research Laboratory, accessed December 2013. [Available online at http://www.esrl.noaa.gov/gmd/ccgg/trends/.]

Thompson, D. W., and Coauthors, 2012: The mystery of recent stratospheric temperature trends. *Nature*, **491**, 692–697, doi:10.1038/nature11579.

Thorne, P. W., and R. S. Vose, 2010: Reanalyses suitable for characterizing long-term trends: Are they really achievable? *Bull. Amer. Meteor. Soc.*, **91**, 353–361, doi:10.1175/2009BAMS2858.1.

Weatherhead, E. C., and Coauthors, 1998: Factors affecting the detection of trends: Statistical considerations and applications to environmental data. *J. Geophys. Res.*, **103**, 17 149–17 161, doi:10.1029/98JD00995.

Zou, C.-Z., and W. Wang, 2009: Diurnal drift correction in the NESDIS/STARMSU/AMSU atmospheric temperature climate data record. *Atmospheric and Environmental Remote Sensing Data Processing and Utilization V: Readiness for FEOSS III*, C.-Z. Zou and W. Wang, Eds., International Society for Optical Engineering (SPIE Proceedings, Vol. 7456), 74560G, doi:10.1117/12.824459.

——, and ——, 2010: Stability of the MSU-derived atmospheric temperature trend. *J. Atmos. Oceanic Technol.*, **27**, 1960–1971, doi:10.1175/2009JTECHA1333.1.

——, and ——, 2011: Intersatellite calibration of AMSU-A observations for weather and climate applications. *J. Geophys. Res.*, **116**, D23113, doi:10.1029/2011JD016205.

——, M. D. Goldberg, Z. Cheng, N. C. Grody, J. T. Sullivan, C. Cao, and D. Tarpley, 2006: Recalibration of microwave sounding unit for climate studies using simultaneous nadir overpasses. *J. Geophys. Res.*, **111**, D19114, doi:10.1029/2005JD006798.